ACS APPLIED ENERGY MATERIALS

www.acsaem.org Article

Electrocatalytic Activity of Oxygen-Functionalized Carbon Electrodes for Vanadium Redox Flow Batteries from Free-Energy Calculations

Zhen Jiang and Vitaly Alexandrov*

Cite This: *ACS Appl. Energy Mater.* 2020, 3, 7543−7549 Read Online

ACCESS | Metrics & More | Article Recommendations

ABSTRACT: Detailed atomistic understanding of the vanadium redox reactions taking place at electrode/water interfaces is key for improvement of the power density of vanadium redox flow batteries. In this work, we employ *ab initio* molecular dynamics-based metadynamics simulations to examine V^{2+}/V^{3+} and VO_2^+/VO^{2+} redox reactions at the oxygen-functionalized graphite $(11\bar{2}0)$ surface contrasting the behavior of O−C═O and C═O groups. By evaluating free-energy barriers, we reveal that the kinetics of adsorption and desorption processes for every vanadium ion is more favorable in the case of O−C═O. We also find that interfacial VO_2^+/VO^{2+} transformations should be more rapid than those observed for the V^{2+}/V^{3+} couple, with the V^{3+} desorption being the rate-limiting step of the overall process. The obtained results suggest that increasing the content of O−C═O groups on carbon-based electrodes should help enhance the power density of vanadium redox flow batteries.

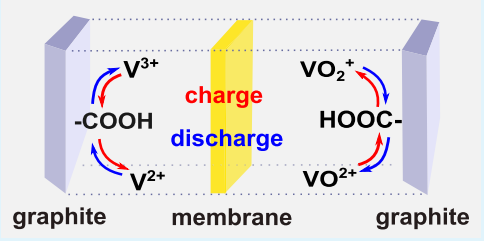

KEYWORDS: *vanadium redox flow batteries, catalytic activity, Car−Parrinello molecular dynamics, carbon electrodes*

1. INTRODUCTION

Rechargeable redox flow batteries (RFBs) have emerged as promising electrochemical energy storage systems for the electric grid powered by the intermittent energy sources such as the sun and wind.[1−5] Aqueous RFBs are considered to be inherently safer and environmentally benign as compared with their organic-based counterparts. Among aqueous RFBs with inorganic redox-active species, all-vanadium RFBs (VRFBs) are the most studied experimentally serving as benchmark systems. Despite significant experimental efforts directed at increasing the energy and power density of aqueous RFBs, the lack of detailed microscopic information about underlying electrochemical reaction mechanisms in RFBs impedes practical progress.

The all-VRFB employs the same chemical element (vanadium) in both half cells to minimize cross-contamination with the following electrochemical reactions occurring in the catholyte and anolyte, respectively

$$VO_2^+ + 2H^+ + e^- \underset{\text{charge}}{\overset{\text{discharge}}{\rightleftharpoons}} VO^{2+} + H_2O, \quad E^0 = 1\ \text{V}\ \textit{versus}\ \text{RHE}$$

$$V^{2+} \underset{\text{charge}}{\overset{\text{discharge}}{\rightleftharpoons}} V^{3+} + e^-, \quad E^0 = -0.26\ \text{V}\ \textit{versus}\ \text{RHE}$$

A common strategy to increase the power density of RFBs is to enhance electrocatalytic activity of electrode materials. In the case of the most cost-effective carbon-based electrodes, a variety of surface treatments has been exploited including thermal,[6] chemical,[7,8] and plasma[9]-based processes. As a result, different functional groups such as oxygen- and nitrogen-based moieties can be introduced to the carbon surface, serving as catalytically active sites for redox reactions at the electrode/electrolyte interface.[10−14] In comparison to pristine carbon, the reactivity and reversibility of such surface-functionalized carbon electrodes can be greatly improved.[15−17]

In the case of all-VRFBs, it was shown that both basal and edge carbon surfaces can be functionalized by oxygen groups such as C−O, C═O, and O−C═O, with the edge surface being more reactive.[13,18] It was also demonstrated that the specific type of oxygen functional group is crucial for tuning the electrocatalytic activity of functionalized carbon electrodes.[19−21] For example, by varying the relative content of different oxygen groups at graphite felt electrodes through plasma treatment, it was suggested that O−C═O should be more electrocatalytically active toward the vanadium redox transformations.[13] Nevertheless, deconvoluting the role of each

Received: April 28, 2020
Accepted: July 9, 2020
Published: July 9, 2020

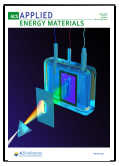

https://dx.doi.org/10.1021/acsaem.0c00972
ACS Appl. Energy Mater. 2020, 3, 7543−7549

specific functional group is challenging because it is experimentally difficult to control the composition of electrode surfaces.

Previously, we have employed Car−Parrinello molecular dynamics (CPMD)-based metadynamics simulations to examine the mechanism and kinetics of interaction between aqueous vanadium species (V^{2+}/V^{3+} and VO^{2+}/VO_2^+) and graphite surfaces functionalized by C═O groups.[22,23] In this work, we aim to extend this investigation by analyzing the interaction between all four vanadium species and the graphite $(11\bar{2}0)$ surface functionalized by O−C═O moieties. This allows us to compare the catalytic behavior of both oxygen functional groups (C═O and O−C═O) within the same computational approach.

2. COMPUTATIONAL DETAILS

Calculations were performed within the plane-wave density functional theory (DFT) framework as implemented in the NWChem code.[24] The exchange and correlation energies were calculated employing the Perdew−Burke−Ernzerhof (PBE) functional within the generalized gradient approximation.[25] The Grimme approach (PBE-D3 with BJ damping) was used to account for van der Waals interactions.[26] The norm-conserving Troullier−Martins pseudopotentials[27] were applied for vanadium, while Hamann pseudopotentials[28,29] were used for oxygen, carbon, and hydrogen. Calculations involving V^{2+}, V^{3+}, VO^{2+}, and VO_2^+ species were performed using the spin-unrestricted formalism. Here, each system was pre-equilibrated, employing quantum mechanics/molecular mechanics (QM/MM) calculations[30] for 6 ps followed by CPMD[31] equilibration for at least 6 ps. All QM/MM and CPMD simulations were carried out using a 12.70 × 13.54 × 14.90 Å box involving the graphite slab and a region of 10 Å between the opposite surfaces containing a vanadium ion (V^{2+}, V^{3+}, VO^{2+}, or VO_2^+) embedded into solution of 53 H_2O molecules to have the water density of approximately 1 g/cm^3 (Figure 1). A Nosé−Hoover thermostat[32,33] was employed to keep the system temperature at around 300 K. CPMD simulations were performed at the Γ-point only. The expansion of the Kohn−Sham electronic wave functions and charge density was done using the kinetic cutoff energies of 60 and 240 Ry, respectively. In all CPMD simulations, hydrogen atoms were replaced with deuterium. A fictitious electronic mass of 600 a.u. and a simulation time step of δt = 5 a.u. (0.121 fs) were set. Atomic configurations from the production CPMD simulations were saved at time intervals of $10\delta t$ and used for further analysis.

Free-energy simulations were performed using the CPMD method in conjunction with metadynamics[34,35] to enhance free-energy landscape sampling associated with vanadium redox reactions at the electrode/water interface. This approach was shown to be successful in estimating activation free-energy barriers for a variety of chemical processes.[23,35−40] In this study, the bond distance between an adsorbing/desorbing vanadium cation and an oxygen atom from the surface O−C═O group was used as the collective variable (CV). To describe the energetics of VO^{2+} deprotonation reaction at the graphite/water interface, the bond distance between the oxygen and a hydrogen atom in one H_2O from the first water shell of VO^{2+} was used as the CV, while to describe protonation energetics of the VO_2^+ adsorbate, an additional proton was moved from the surface COOH to the aqueous solution to form H_3O^+. In all metadynamics simulations, the height and width of repulsive

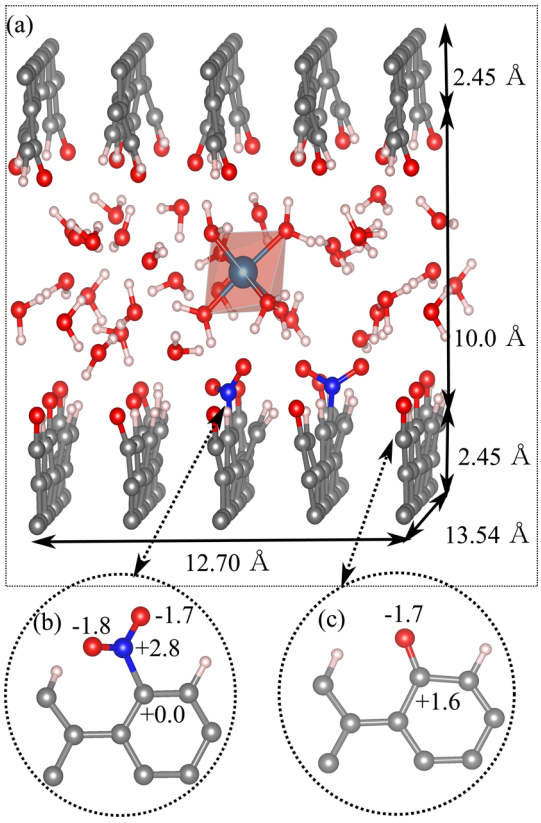

Figure 1. (a) Simulation cell used to model redox reactions for aqueous V^{2+}/V^{3+} and VO^{2+}/VO_2^+ couples at O−C═O sites on the graphite edge $(11\bar{2}0)$ surface. The calculated Bader charges on the atoms of the O−C═O and C═O groups are shown in (b,c), respectively.

Gaussian hills were chosen to be 0.001 and 0.1 a.u., respectively, and were added to the potential every $100\delta t$.

In our previous work, we have employed a graphite edge $(11\bar{2}0)$ surface as a model for carbon-based electrodes and functionalized the surface with C═O/C−H groups in a ratio of 1:2 resulting from complete water dissociation.[23] The vanadium redox reactions were then simulated at the C═O sites of the graphite surface.[23] In this study, we employ a similar structural model introducing two O−C═O groups to the surface that replace two C═O groups at the adjacent graphite layers as shown in Figure 1. This allows us to examine vanadium adsorption/desorption processes in both single-site and double-site binding modes. We found that the protons from the surface carboxylic groups spontaneously diffused into solution during CPMD equilibration, leaving behind O−C═O considered in our simulations.

The Bader charge analysis was performed using structural snapshots extracted from the corresponding CPMD trajectories to evaluate the charge states of vanadium ions. A similar DFT approach was previously undertaken to study properties of vanadium ions in aqueous solutions,[41,42] membranes,[43,44] and at the graphite/water interfaces.[22,23] The charge neutrality of simulation cells was ensured by deleting two protons from the surface carboxyl groups in the case of V^{2+} and VO^{2+}, one proton in the case of VO_2^+, and three protons (two from carboxyl groups and one from the surface C−H group on the opposite side of the slab) when modeling V^{3+}.

https://dx.doi.org/10.1021/acsaem.0c00972
ACS Appl. Energy Mater. 2020, 3, 7543−7549

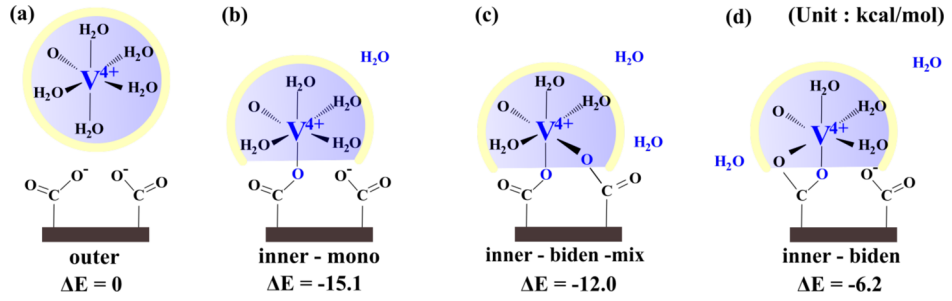

Figure 2. Binding energetics for aqueous VO^{2+} adsorbing from the outer-sphere adsorption configuration (a), taken as a reference, as the inner-sphere monodentate complex (b), inner-sphere bidentate at two O−C═O groups (c), and inner-sphere bidentate at one O−C═O group (d) of the functionalized graphite $(11\bar{2}0)$ surface.

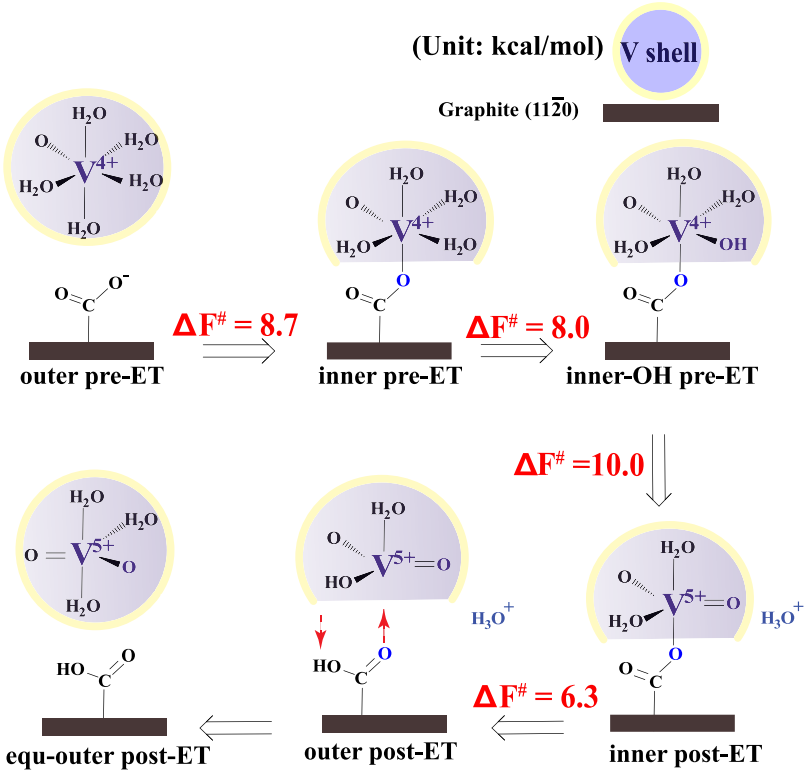

Figure 3. Schematic showing the reaction mechanism of $VO^{2+} \rightarrow VO_2^+$ redox transformation at the O−C═O site of the graphite edge $(11\bar{2}0)$ surface and associated free-energy barriers calculated using CPMD metadynamics. Pre- and post-ET stand for VO^{2+} species before electron transfer (ET and for VO_2^+ after ET has occurred, respectively.

3. RESULTS AND DISCUSSION

3.1. $VO^{2+} \rightarrow VO_2^+$ (Charging). In this section, we focus on the oxidation of aqueous VO^{2+} to VO_2^+ occurring at the electrode surface during the charging process. First of all, we demonstrate that the inner-sphere monodentate adsorption configuration of VO^{2+} is the most energetically favorable adsorption state according to static DFT calculations with the thermodynamic driving force of about −15 kcal/mol relative to the outer-sphere state (see Figure 2). The inner-sphere complex adsorbed in the bidentate configuration involving two neighboring surface O−C═O groups (Figure 2c) turns out to be slightly less stable, while the complex bidentately attached to the same O−C═O group (Figure 2d) is estimated to be much less stable.

As configurations (b) and (c) are found to be almost equally stable in static DFT, we next evaluate the activation free-energy barriers associated with adsorption of VO^{2+} from configuration (a) to both (b) and (c) through CPMD metadynamics. By using the bond distance between V and O of the surface O−C═O group as a CV for the (a) → (b) process, we estimate the activation barrier of about 8.7 kcal/mol (see Figure 3). To sample (a) → (c) adsorption pathway, we chose the bond distances between V and two Os (from neighboring O−C═O groups) as CVs; however, we observed that the monodentate configuration (b) is first formed, while configuration (c) was not formed even for the accumulated external potential greater than 30 kcal/mol. At this point, the simulation was terminated as the activation barrier was deemed to be high. This is similar to our computational results previously obtained for the C═O groups where adsorption of VO^{2+} onto two surface C═O groups was found to be unfavorable.[23] Therefore, we consider the monodentate configuration (b) as the most probable adsorption state for VO^{2+}. Thus, similarly to our previous work on the graphite surface functionalized by C═O groups, we

https://dx.doi.org/10.1021/acsaem.0c00972
ACS Appl. Energy Mater. 2020, 3, 7543−7549

Table 1. Bader Charges q, Magnetic Moments m, and Interpreted Vanadium Oxidation States for Reaction Intermediates in the $VO^{2+} \rightarrow VO_2^+$ Redox Reaction Pathway Shown in Figure 3[a]

	outer pre-ET	inner pre-ET	inner pre-ET-OH	inner post-ET	outer post-ET	equ-outer post-ET
q (V shell), e	1.67	1.53	0.95	0.74	0.03	1.11
q (V), e	2.27	2.28	2.27	2.45	2.39	2.45
m (V), μ_B	1.22	1.24	1.22	0.0	0.0	0.0
oxidation state (V)	+4	+4	+4	+5	+5	+5

[a] q (V shell) stands for the charge on a vanadium cation including species from its first coordination sphere.

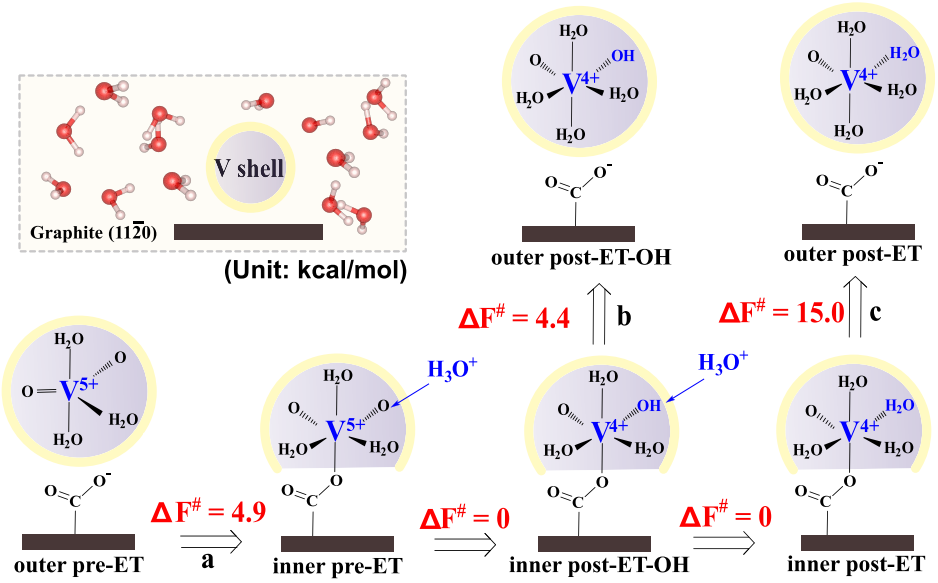

Figure 4. Schematic showing the mechanisms of $VO_2^+ \rightarrow VO^{2+}$ redox reaction at the O−C═O site of the graphite edge (11$\bar{2}$0) surface and associated free-energy barriers calculated using CPMD metadynamics. Pre- and post-ET stand for VO^{2+} species before ET and for VO_2^+ after ET has occurred, respectively.

carry out CPMD analysis focusing only on the inner-sphere monodentate adsorption configurations.

Figure 3 schematically shows the mechanism of the $VO^{2+} \rightarrow VO_2^+$ redox reaction with the corresponding activation free-energy barriers of adsorption/desorption estimated through metadynamics simulations. It is seen that following the first adsorption step (from outer pre-ET to inner pre-ET), two subsequent deprotonation events of an H_2O ligand in the first hydration shell of VO^{2+} occur, each characterized by 8.0 and 10.0 kcal/mol barriers to produce the VO_2^+ adsorbate. According to the Bader charge and magnetic moment analysis (Table 1), the ET for $VO^{2+} \rightarrow VO_2^+$ transformation is found to be coupled to the second deprotonation step (from inner-OH pre-ET to inner post-ET complex), where the magnetic moment of the vanadium ion decreases from 1.22 to 0 μ_B. Finally, the desorption of the inner post-ET VO_2^+ complex back into aqueous solution takes place with a 6.3 kcal/mol free-energy barrier that is also coupled to one proton transfer from aqueous VO_2^+ to the surface O−C═O group.

Overall, we determine that the kinetics of VO^{2+} adsorption and VO_2^+ desorption is more favorable for O−C═O than for C═O. Specifically, the free-energy barriers for VO^{2+} adsorption and VO_2^+ desorption are evaluated to be 9 and 6 kcal/mol, respectively, which is lower than in the case of O−C═O group. Also, the barriers for two deprotonation reactions accompanying ET are slightly decreased (by ∼2 kcal/mol) in the case of O−C═O due to its participation in the proton exchange.

3.2. $VO_2^+ \rightarrow VO^{2+}$ (Discharging). We next examine the reverse process of VO_2^+ reduction to VO^{2+} that takes place upon the battery discharge. Figure 4 shows the redox reaction mechanism with the free-energy barriers evaluated for all reaction steps. The first step is the adsorption of aqueous VO_2^+ to the O−C═O site on the graphite surface from the outer- to inner-sphere adsorbate configuration yielding a barrier of 4.9 kcal/mol. Again, this barrier is significantly smaller than the one obtained for the C═O group[23] (11.7 kcal/mol). Given the acidic pH common to aqueous VRFBs, we next consider the effect of extra protons present in solution. Our CPMD simulations reveal that if extra H_3O^+ ions are sequentially placed in the immediate vicinity of the adsorbed VO_2^+ ion (inner pre-ET complex in Figure 4), one of the two O atoms in VO_2^+ will become spontaneously protonated into OH and then H_2O, leading to the formation of surface−bound complexes depicted as inner post-ET-OH and inner post-ET in Figure 4, respectively. By modeling desorption of both complexes from the surface O−C═O group, we identify that the detachment of the inner-sphere post-ET complex is an energetically more intensive process (15.0 kcal/mol) than that of the inner-sphere post-ET-OH complex (4.4 kcal/mol). As we observed that the breaking of the V−OOC bond can be facilitated by protonation of the adjacent O atom belonging to the same O−C═O group, we also consider this reaction pathway. Our estimate of the corresponding activation barrier provides a value greater than 10.0 kcal/mol, which is higher than the direct detachment of V^{4+} (with an activation barrier of 4.4 kcal/mol shown in Figure 4).

https://dx.doi.org/10.1021/acsaem.0c00972
ACS Appl. Energy Mater. 2020, 3, 7543−7549

Table 2. Bader Charges q, Magnetic Moments m, and Interpreted Vanadium Oxidation States for Reaction Intermediates in the $VO_2^+ \rightarrow VO^{2+}$ Redox Reaction Pathway Shown in Figure 4[a]

	outer pre-ET	inner pre-ET	inner post-ET-OH	outer post-ET-OH	inner post-ET	outer post-ET
q (V shell), e	1.11	0.74	0.95	1.08	1.53	1.67
q (V), e	2.45	2.45	2.27	2.27	2.27	2.28
m (V), μ_B	0.0	0.0	1.24	1.24	1.22	1.22
oxidation state (V)	+5	+5	+4	+4	+4	+4

[a] q (V shell) stands for the charge on a vanadium cation including species from its first coordination sphere.

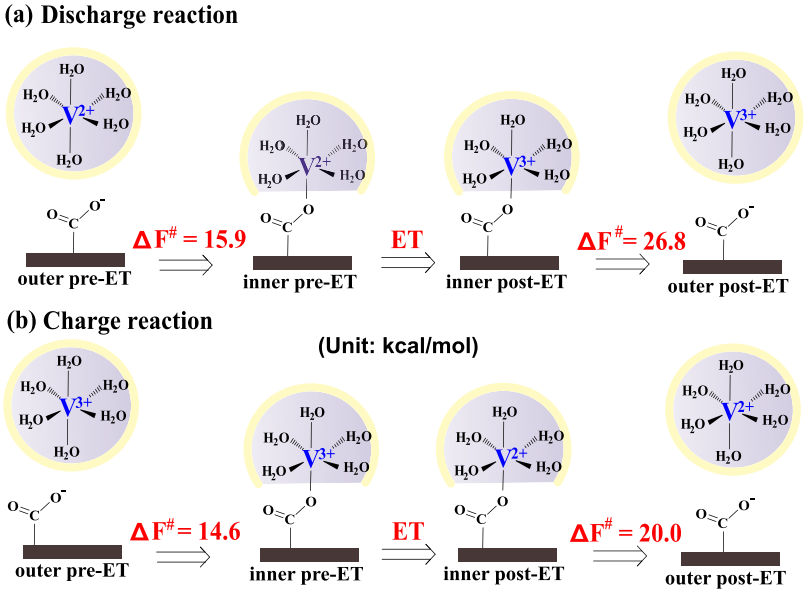

Figure 5. Schematic showing the mechanisms of $V^{2+} \rightleftharpoons V^{3+}$ redox reaction at the O−C═O site of the graphite edge $(11\bar{2}0)$ surface and associated free-energy barriers calculated using CPMD metadynamics.

Table 2 presents the DFT-calculated Bader atomic charges (q) and magnetic moments (m) for all reaction intermediates shown in Figure 4. It is clearly seen that all pre-ET complexes representing adsorbing V^{5+} species have q and m values of 2.45 e and 0 μ_B, respectively, confirming the 5+ oxidation state of vanadium. Post-ET complexes are characterized by ∼1.23 μ_B magnetic moment and 2.27 e Bader charge on the vanadium species indicative of the 4+ oxidation state of vanadium. It is also seen that the Bader charge of the whole outer-sphere post-ET vanadium complex (1.67 e) is close to the formal 2+ charge of VO^{2+}. In general, the interpretation of vanadium oxidation states is more apparent from the difference of magnetic moments than from the computed Bader charges. The observed greater sensitivity of magnetic moments than ionic charges to the ET process appears to be in agreement with other computational studies.[45,46] As for the distances between the adsorbed vanadium and surface oxygen ions, they also agree with the assigned oxidation states being about 1.99 Å for V^{5+}−O *versus* 2.14 Å for V^{4+}−O when averaged over the CPMD trajectories.

3.3. $V^{2+} \rightleftharpoons V^{3+}$. Contrary to the mechanism of the interfacial VO^{2+}/VO_2^+ redox reactions, the V^{2+}/V^{3+} reactions do not include an ion exchange process. As shown in Figure 5, the discharge process starts from the adsorption of aqueous V^{2+} onto the O atom of the surface COO site, followed by ET from adsorbed V to the electrode through the formed C−O−V bond, after which V^{3+} will desorb back into the bulk solution. The process is reversed upon charging.

Figure 5 shows V^{2+}/V^{3+} reactions at the carboxylated graphite edge surface with the corresponding free-energy barriers estimated from CPMD-based metadynamics simulations. Similarly to the V^{2+}/V^{3+} redox reactions on the C═O sites,[23] the rate-determining step is the desorption of V^{3+} ion with the activation barriers estimated at 26.8 kcal/mol, while the desorption of V^{2+} ion exhibits a lower activation barrier of 20.0 kcal/mol, in agreement with stronger electrostatic attraction of V^{3+} to the surface. The adsorption processes for V^{2+} and V^{3+} are characterized by the barriers of 15.9 and 14.6 kcal/mol, respectively, also in accordance with expectations from electrostatics. The results indicate V^{3+} desorption as the slowest process in the overall reaction with the free-energy barriers being systematically lower than those obtained for the graphite edge functionalized by the C═O groups.

Finally, we also analyze the intrinsic errors associated with the application of CPMD metadynamics approach to evaluate free-energy barriers. The employed method has been previously used in a number of computational studies where more details on the approach can be found.[23,34,35,40] Table 3 lists the computed activation free-energies for all examined reactions together with estimated errors. Overall, the errors are in the range between 0.7 and 3.6 kcal/mol depending on the reaction and do not change the conclusions drawn above.

4. CONCLUSIONS

In this study, we performed DFT calculations within the CPMD metadynamics approach to evaluate free-energy barriers associated with the V^{2+}/V^{3+} and VO_2^+/VO^{2+} redox

https://dx.doi.org/10.1021/acsaem.0c00972
ACS Appl. Energy Mater. 2020, 3, 7543−7549

Table 3. Summary of the Free-Energy Barriers Obtained from metadynamics along with Estimated Errors for All Adsorption ($\Delta F_1^{\#}$), Protonation/Deprotonation ($\Delta F_2^{\#}$ and $\Delta F_3^{\#}$) and Desorption ($\Delta F_4^{\#}$) Steps of $VO^{2+} \rightarrow VO_2^{+}$ (Figure 3), $VO_2^{+} \rightarrow VO^{2+}$ (Figure 4), and $V^{2+} \rightleftharpoons V^{3+}$ (Figure 5) Reactions at the O−C═O Site of the Graphite Edge Surface (in kcal/mol)

reaction	$\Delta F_1^{\#}$	$\Delta F_2^{\#}$	$\Delta F_3^{\#}$	$\Delta F_4^{\#}$
$VO^{2+} \rightarrow VO_2^{+}$	8.7 ± 3.6	8.0 ± 0.7	10.0 ± 0.7	6.3 ± 2.3
$VO_2^{+} \rightarrow VO^{2+}$	4.9 ± 2.5	0	0	4.4 ± 2.1; 15.0 ± 0.7
$V^{2+} \rightarrow V^{3+}$	15.9 ± 1.9			26.8 ± 3.1
$V^{3+} \rightarrow V^{2+}$	14.6 ± 1.6			20.0 ± 2.6

reactions at the oxygen-functionalized graphite surface relevant to all-VRFBs. Specifically, we analyzed the catalytic role of carboxylic (O−C═O) groups at the graphite edge $(11\bar{2}0)$ surface and compared it with the results previously obtained for the C═O groups. We determined that for both oxygen functional groups, the most favorable mode of vanadium adsorption is the monodentate inner-sphere adsorption configuration. We found that both adsorption and desorption processes are systematically more facile for each of the four aqueous vanadium species (VO_2^{+}, VO^{2+}, V^{3+}, and V^{2+}) at the graphite surface modified by the O−C═O groups. One of the reasons for a relatively fast desorption of VO_2^{+} from the O−C═O site was found to be the proton exchange between an O ion of the surface group and an H_2O ligand of the VO_2^{+} ion. It was estimated that all activation barriers for the discharge reaction in the catholyte (VO_2^{+}/VO^{2+}) at the O−C═O site are less than 5 kcal/mol, while desorption of V^{3+} in the anolyte was found to be the rate-determining step with a barrier of about 27 kcal/mol. The present study provides atomistic insights into the vanadium adsorption/desorption kinetics for each type of oxygen functional group at the graphite electrode that is challenging to pinpoint experimentally.

AUTHOR INFORMATION

Corresponding Author

Vitaly Alexandrov − *Department of Chemical and Biomolecular Engineering and Nebraska Center for Materials and Nanoscience, University of Nebraska−Lincoln, Lincoln, Nebraska 68588, United States;* orcid.org/0000-0003-2063-6914; Phone: +1 402 4725323; Email: valexandrov2@unl.edu

Author

Zhen Jiang − *Department of Chemical and Biomolecular Engineering, University of Nebraska−Lincoln, Lincoln, Nebraska 68588, United States;* orcid.org/0000-0002-1175-5658

Complete contact information is available at: https://pubs.acs.org/10.1021/acsaem.0c00972

Notes

The authors declare no competing financial interest.

ACKNOWLEDGMENTS

The Holland Computing Center at the University of Nebraska−Lincoln is acknowledged for computational support.

REFERENCES

(1) Noack, J.; Roznyatovskaya, N.; Herr, T.; Fischer, P. The Chemistry of Redox-Flow Batteries. *Angew. Chem., Int. Ed.* **2015**, *54*, 9776−9809.

(2) Soloveichik, G. L. Flow Batteries: Current Status and Trends. *Chem. Rev.* **2015**, *115*, 11533−11558.

(3) Park, M.; Ryu, J.; Wang, W.; Cho, J. Material Design and Engineering of Next-Generation Flow-Battery Technologies. *Nat. Rev. Mater.* **2016**, *2*, 16080.

(4) Wei, X.; Pan, W.; Duan, W.; Hollas, A.; Yang, Z.; Li, B.; Nie, Z.; Liu, J.; Reed, D.; Wang, W.; Sprenkle, V. Materials and Systems for Organic Redox Flow Batteries: Status and Challenges. *ACS Energy Lett.* **2017**, *2*, 2187−2204.

(5) Kamat, P. V.; Schanze, K. S.; Buriak, J. M. Redox Flow Batteries. *ACS Energy Lett.* **2017**, *2*, 1368−1369.

(6) Sun, B.; Skyllas-Kazacos, M. Modification of Graphite Electrode Materials for Vanadium Redox Flow Battery Application-I. Thermal Treatment. *Electrochim. Acta* **1992**, *37*, 1253−1260.

(7) Sun, B.; Skyllas-Kazacos, M. Chemical Modification of Graphite Electrode Materials for Vanadium Redox Flow Battery Application—part II. Acid Treatments. *Electrochim. Acta* **1992**, *37*, 2459−2465.

(8) Xia, L.; Zhang, Q.; Wu, C.; Liu, Y.; Ding, M.; Ye, J.; Cheng, Y.; Jia, C. Graphene Coated Carbon Felt as a High-Performance Electrode for All Vanadium Redox Flow Batteries. *Surf. Coat. Technol.* **2019**, *358*, 153−158.

(9) Dixon, D.; Babu, D. J.; Langner, J.; Bruns, M.; Pfaffmann, L.; Bhaskar, A.; Schneider, J. J.; Scheiba, F.; Ehrenberg, H. Effect of Oxygen Plasma Treatment on the Electrochemical Performance of the Rayon and Polyacrylonitrile Based Carbon Felt for the Vanadium Redox Flow Battery Application. *J. Power Sources* **2016**, *332*, 240−248.

(10) Kim, S.-C.; Lim, H.; Kim, H.; Yi, J. S.; Lee, D. Nitrogen and Oxygen Dual-doping on Carbon Electrodes by Urea Thermolysis and Its Electrocatalytic Significance for Vanadium Redox Flow Battery. *Electrochim. Acta* **2020**, *348*, 136286.

(11) Yoon, S. J.; Kim, S.; Kim, D. K.; So, S.; Hong, Y. T.; Hempelmann, R. Ionic Liquid Derived Nitrogen Doped Graphite Felt Electrodes for Vanadium Redox Flow Batteries. *Carbon* **2020**, *166*, 131−137.

(12) Liu, T.; Li, X.; Xu, C.; Zhang, H. Activated Carbon Fiber Paper Based Electrodes with High Electrocatalytic Activity for Vanadium Flow Batteries with Improved Power Density. *ACS Appl. Mater. Interfaces* **2017**, *9*, 4626−4633.

(13) Estevez, L.; Reed, D.; Nie, Z.; Schwarz, A. M.; Nandasiri, M. I.; Kizewski, J. P.; Wang, W.; Thomsen, E.; Liu, J.; Zhang, J.-G.; Sprenkle, V.; Li, B. Tunable Oxygen Functional Groups as Electrocatalysts on Graphite Felt Surfaces for All-Vanadium Flow Batteries. *ChemSusChem* **2016**, *9*, 1455−1461.

(14) Yu, L.; Lin, F.; Xiao, W.; Xu, L.; Xi, J. Achieving Efficient and Inexpensive Vanadium Flow Battery by Combining $Ce_xZr_{1-x}O_2$ Electrocatalyst and Hydrocarbon Membrane. *Chem. Eng. J.* **2019**, *356*, 622−631.

(15) Kim, K. J.; Park, M.-S.; Kim, Y.-J.; Kim, J. H.; Dou, S. X.; Skyllas-Kazacos, M. A Technology Review of Electrodes and Reaction Mechanisms in Vanadium Redox Flow Batteries. *J. Mater. Chem. A* **2015**, *3*, 16913−16933.

(16) Fink, H.; Friedl, J.; Stimming, U. Composition of the Electrode Determines Which Half-Cell's Rate Constant is Higher in a Vanadium Flow Battery. *J. Phys. Chem. C* **2016**, *120*, 15893−15901.

(17) Pour, N.; Kwabi, D. G.; Carney, T.; Darling, R. M.; Perry, M. L.; Shao-Horn, Y. Influence of Edge- and Basal-Plane Sites on the Vanadium Redox Kinetics for Flow Batteries. *J. Phys. Chem. C* **2015**, *119*, 5311−5318.

(18) Jiang, Y.; Cheng, G.; Li, Y.; He, Z.; Zhu, J.; Meng, W.; Zhou, H.; Dai, L.; Wang, L. Superior Electrocatalytic Performance of Porous, Graphitic, and Oxygen-Functionalized Carbon Nanofiber as Bifunctional Electrode for Vanadium Redox Flow Battery. *Appl. Surf. Sci.* **2020**, *525*, 146453.

(19) Li, W.; Liu, J.; Yan, C. Graphite-graphite oxide composite electrode for vanadium redox flow battery. *Electrochim. Acta* **2011**, *56*, 5290−5294.
(20) Li, W.; Liu, J.; Yan, C. Multi-walled Carbon Nanotubes Used as an Electrode Reaction Catalyst for VO_2^+/VO^{2+} for a Vanadium Redox Flow Battery. *Carbon* **2011**, *49*, 3463−3470.
(21) Li, Y.; Parrondo, J.; Sankarasubramanian, S.; Ramani, V. Impact of Surface Carbonyl- and Hydroxyl-Group Concentrations on Electrode Kinetics in an All-Vanadium Redox Flow Battery. *J. Phys. Chem. C* **2019**, *123*, 6370−6378.
(22) Jiang, Z.; Klyukin, K.; Alexandrov, V. First-principles Study of Adsorption-Desorption Kinetics of Aqueous V^{2+}/V^{3+} Redox Species on Graphite in a Vanadium Redox Flow Battery. *Phys. Chem. Chem. Phys.* **2017**, *19*, 14897−14901.
(23) Jiang, Z.; Klyukin, K.; Alexandrov, V. Ab Initio Metadynamics Study of the VO_2^+/VO^{2+} Redox Reaction Mechanism at the Graphite Edge/Water Interface. *ACS Appl. Mater. Interfaces* **2018**, *10*, 20621−20626.
(24) Valiev, M.; Bylaska, E. J.; Govind, N.; Kowalski, K.; Straatsma, T. P.; Van Dam, H. J. J.; Wang, D.; Nieplocha, J.; Apra, E.; Windus, T. L.; de Jong, W. A. NWChem: a Comprehensive and Scalable Open-Source Solution for Large Scale Molecular Simulations. *Comput. Phys. Commun.* **2010**, *181*, 1477−1489.
(25) Perdew, J. P.; Burke, K.; Ernzerhof, M. Generalized Gradient Approximation Made Simple. *Phys. Rev. Lett.* **1996**, *77*, 3865.
(26) Grimme, S.; Ehrlich, S.; Goerigk, L. Effect of the Damping Function in Dispersion Corrected Density Functional Theory. *J. Comput. Chem.* **2011**, *32*, 1456−1465.
(27) Troullier, N.; Martins, J. L. Efficient Pseudopotentials for Plane-Wave Calculations. *Phys. Rev. B: Condens. Matter Mater. Phys.* **1991**, *43*, 1993.
(28) Hamann, D. R.; Schlüter, M.; Chiang, C. Norm-Conserving Pseudopotentials. *Phys. Rev. Lett.* **1979**, *43*, 1494.
(29) Hamann, D. R. Generalized Norm-Conserving Pseudopotentials. *Phys. Rev. B: Condens. Matter Mater. Phys.* **1989**, *40*, 2980.
(30) Cauët, E.; Bogatko, S.; Weare, J. H.; Fulton, J. L.; Schenter, G. K.; Bylaska, E. J. Structure and Dynamics of the Hydration Shells of the Zn^{2+} Ion from ab Initio Molecular Dynamics and Combined ab Initio and Classical Molecular Dynamics Simulations. *J. Chem. Phys.* **2010**, *132*, 194502.
(31) Car, R.; Parrinello, M. Unified Approach for Molecular Dynamics and Density-Functional Theory. *Phys. Rev. Lett.* **1985**, *55*, 2471.
(32) Nosé, S. A Molecular Dynamics Method for Simulations in the Canonical Ensemble. *Mol. Phys.* **1984**, *52*, 255−268.
(33) Hoover, W. G. Canonical Dynamics: Equilibrium Phase-Space Distributions. *Phys. Rev. B: Condens. Matter Mater. Phys.* **1985**, *31*, 1695.
(34) Bussi, G.; Laio, A.; Parrinello, M. Equilibrium Free Energies from Nonequilibrium Metadynamics. *Phys. Rev. Lett.* **2006**, *96*, 090601.
(35) Laio, A.; Gervasio, F. L. Metadynamics: a Method to Simulate Rare Events and Reconstruct the Free Energy in Biophysics, Chemistry and Material Science. *Rep. Prog. Phys.* **2008**, *71*, 126601.
(36) Stirling, A.; Pápai, I. H_2CO_3 Forms via HCO_3^- in Water. *J. Phys. Chem. B* **2010**, *114*, 16854−16859.
(37) Stirling, A. HCO_3^--Formation from CO_2 at High pH: Ab Initio Molecular Dynamics Study. *J. Phys. Chem. B* **2011**, *115*, 14683−14687.
(38) Cheng, T.; Xiao, H.; Goddard, W. A., III Reaction Mechanisms for the Electrochemical Reduction of CO_2 to CO and Formate on the Cu (100) Surface at 298 K from Quantum Mechanics Free Energy Calculations with Explicit Water. *J. Am. Chem. Soc.* **2016**, *138*, 13802−13805.
(39) Klyukin, K.; Alexandrov, V. CO_2 Adsorption and Reactivity on Rutile TiO2 (110) in Water: An Ab Initio Molecular Dynamics Study. *J. Phys. Chem. C* **2017**, *121*, 10476−10483.
(40) Jiang, Z.; Klyukin, K.; Miller, K.; Alexandrov, V. Mechanistic Theoretical Investigation of Self-Discharge Reactions in a Vanadium Redox Flow Battery. *J. Phys. Chem. B* **2019**, *123*, 3976−3983.
(41) Jiang, Z.; Klyukin, K.; Alexandrov, V. Structure, Hydrolysis, and Diffusion of Aqueous Vanadium Ions from Car-Parrinello Molecular Dynamics. *J. Chem. Phys.* **2016**, *145*, 114303.
(42) Bon, M.; Laino, T.; Curioni, A.; Parrinello, M. Characterization of Vanadium Species in Mixed Chloride-Sulfate Solutions: An Ab Initio Metadynamics Study. *J. Phys. Chem. C* **2016**, *120*, 10791−10798.
(43) Nibel, O.; Bon, M.; Agiorgousis, M. L.; Laino, T.; Gubler, L.; Schmidt, T. J. Unraveling the Interaction Mechanism between Amidoxime Groups and Vanadium Ions at Various pH Conditions. *J. Phys. Chem. C* **2017**, *121*, 6436−6445.
(44) Intan, N. N.; Klyukin, K.; Zimudzi, T. J.; Hickner, M. A.; Alexandrov, V. A Combined Theoretical-Experimental Study of Interactions between Vanadium Ions and Nafion Membrane in All-Vanadium Redox Flow Batteries. *J. Power Sources* **2018**, *373*, 150−160.
(45) Xu, M.; Xiao, P.; Stauffer, S.; Song, J.; Henkelman, G.; Goodenough, J. B. Theoretical and Experimental Study of Vanadium-Based Fluorophosphate Cathodes for Rechargeable Batteries. *Chem. Mater.* **2014**, *26*, 3089−3097.
(46) Leung, K. First-Principles Modeling of Mn(II) Migration above and Dissolution from $Li_xMn_2O_4$ (001) Surfaces. *Chem. Mater.* **2017**, *29*, 2550−2562.

https://dx.doi.org/10.1021/acsaem.0c00972
ACS Appl. Energy Mater. 2020, 3, 7543−7549